

Delocalized polaron and Burstein-Moss shift induced by Li in α -V₂O₅: A DFT + DMFT studyHuu T. Do ^{1,2,*}, Alex Taekyung Lee ^{1,2,*}, Hyowon Park,^{2,3} and Anh T. Ngo^{1,2,†}¹Department of Chemical Engineering, University of Illinois, Chicago, Illinois 60607, USA²Materials Science Division, Argonne National Laboratory, Argonne, Illinois 60439, USA³Department of Physics, University of Illinois, Chicago, Illinois 60607, USA (Received 8 August 2023; revised 15 October 2023; accepted 19 October 2023; published 13 November 2023)

We performed density functional theory (DFT)+ U and dynamical mean field theory (DMFT) calculations with a continuous-time quantum Monte Carlo impurity solver to investigate the electronic properties of V₂O₅ and Li_{*x*}V₂O₅ ($x = 0.125$ and 0.25). Pristine V₂O₅ is a charge-transfer insulator with strong O p -V d hybridization, and it exhibits a large band gap (E_{gap}) as well as a nonzero conduction-band (CB) gap. We show that the band gap, the number of d electrons of vanadium, N_d , and the CB gap for V₂O₅ obtained from our DMFT calculations are in excellent agreement with the experimental values. While the DFT + U approach replicates the experimental band gap, it overestimates the value of N_d and underestimates the CB gap. In the presence of low Li doping, the electronic properties of V₂O₅ are mainly driven by a polaronic mechanism, and electron spin resonance and electron nuclear double resonance spectroscopies observed the coexistence of free and bound polarons. Notably, our DMFT results identify both polaron types, with the bound polaron being energetically preferred, while the DFT + U method only predicts the free polaron. Our DMFT analysis also reveals that increased Li doping leads to electron filling in the conduction band, shifting the Fermi level. This result is consistent with the observed Burstein-Moss shift upon enhanced Li doping, and we thus demonstrate that the DFT + DMFT approach can be used for an accurate and realistic description of strongly correlated materials.

DOI: [10.1103/PhysRevB.108.205122](https://doi.org/10.1103/PhysRevB.108.205122)**I. INTRODUCTION**

Vanadium pentoxide (V₂O₅) is an interesting compound in the vanadium-oxide family, since its highest oxidation state +5 (d^0) results in the strongest degree of electronegativity and the largest percentage of covalent bonds in oxide compounds, and it can be easily reduced to lower oxidation states [1,2]. Furthermore, V₂O₅ has long been an attractive exemplar for both the fundamental research of electronic properties in transition oxides [3–6] and a variety of applications in photocatalysis, and for smart windows, especially in fabricating a cathode for electrochemical storage [7–12].

V₂O₅ exists in several polymorphs, such as α , β , γ' phases [13,14], and the α phase is the most stable at ambient conditions. α -V₂O₅ has a layered structure (Fig. 1) with orthorhombic space group ($Pmmn$), and the layers interact with each other via a weak van der Waals force [15–17]. α -V₂O₅ is a charge-transfer insulator, and it has band gap of 2.3–2.8 eV [7,18–20]. There is also a gap in the conduction band (CB) around 0.5 eV separating between the split-off band and the main conduction band [6] (see Fig. 2). The number of electrons in the V d manifold (N_d) was also measured experimentally. Though V is in a d^0 state, N_d shows a nonzero value due to the strong O p -V d hybridization. Resonant photoemission spectroscopy (RPES) estimated $N_d = 2.0$ for

V₂O₅ [21], while the cluster model predicted $N_d = 1.2$ based on XPS and x-ray absorption spectroscopy (XAS) [22].

Previous DFT + U studies suggested a band gap of 1.5–2.2 eV, while the CB gap is only 0–0.15 eV [12,23,24]. This value is much smaller than the experimental value of 0.4–0.5 eV. Recent GW results showed that both the band gap and the CB gap are increased to 2.4 and 0.3 eV, respectively. However, to our knowledge, N_d values have not been reported in past first-principles studies. Since N_d represents the strength of the p - d hybridization, and because V₂O₅ is a charge-transfer insulator, N_d plays a crucial role in deciphering the electronic properties of V₂O₅.

Due to the layer-by-layer structure, α -V₂O₅ promises a potential candidate for the cathode material of an Li-battery by intercalating Li⁺ ions between layers, particularly for rechargeable microbatteries due to very high specific densities and capacities [25,26]. Depending on the Li ratio, several phases of Li_{*x*}V₂O₅ are observed: α ($x \leq 0.1$), ϵ ($0.33 \leq x \leq 0.64$), or δ ($0.7 \leq x \leq 1.0$) phases [27–30].

Li atoms in Li_{*x*}V₂O₅ donate electrons to V d bands and becomes Li⁺ ions. With Li-doping, the electronic properties of α -Li_{*x*}V₂O₅ are changed unexpectedly during the lithiation process. If the Li concentration is low ($x = 0.001$ and 0.005), two types of polarons are observed experimentally: (i) free polarons localized at single V sites, and (ii) bound polarons delocalized over four V sites around a Li⁺ ion [31,32]. On the other hand, as x increases, the optical band gap is increased with Li doping, which indicates the Burstein-Moss shift, i.e., the Fermi level is shifted due to the doped electron in the conduction band [6].

*These authors contributed equally to this work.

†anhngo@uic.edu

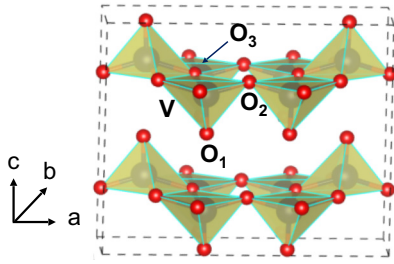


FIG. 1. Crystal structure of pristine α - V_2O_5 , which includes two layers ($1 \times 2 \times 1$ supercell).

There are several DFT + U studies of $Li_xV_2O_5$ in the literature, and they showed that the doped electron occupies the defect level located at the middle of the band gap, while the conduction band is empty [12,23,33,34]. In these cases, the defect level or the electron is spatially localized on a single V site, similar to the free polaron, with a migration barrier of 0.12–0.34 eV. [33,34]. However, the bound polaron has not been found by DFT + U studies. In addition, since the electron occupies the defect level, there is no shift of the Fermi level within DFT + U .

In this work, we investigate the electronic structures of V_2O_5 and $Li_xV_2O_5$ ($x = 0.125$ and 0.25) using both DFT + U and DFT + DMFT methods. We show that N_d of V_2O_5 within DFT + U is approximately twice the experimental value, and N_d using the dynamical mean field theory (DMFT) method is similar to the experimental value. We find that the bound polaron, where an electron is delocalized over four V sites, is energetically more stable than the free polaron within DMFT for $Li_{0.125}V_2O_5$. Moreover, we show that as x increases, the defect level is empty and an electron occupies the conduction band within DMFT. This result is consistent with the Fermi level shift or Burstein-Moss effect in the experiments [6,25].

We organize our manuscript as follows. Section II describes in detail the optimization of crystal structure and electronic calculations using DFT + U and DFT + DMFT.

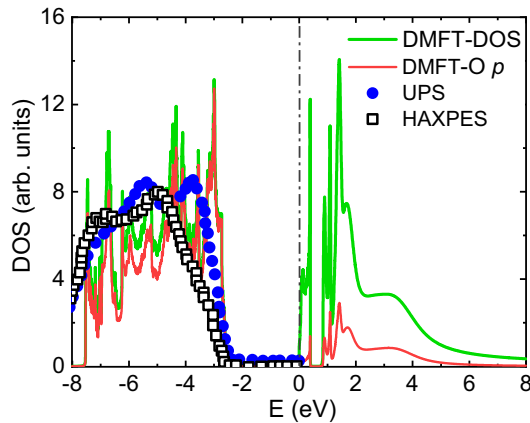


FIG. 2. DOS from experiments and DFT + DMFT. There is a gap in the conduction band (CB gap). We use ultraviolet photoemission spectroscopy (UPS) data with photon energies of 32 eV in Ref. [4], and hard x-ray photoemission spectroscopy (HAXPES) data in Ref. [12]. Here, all experiments were measured at room temperature. The parameters for DMFT calculation are set by $U = 5.5$ eV, $J = 0.5$ eV, $\lambda = 0.4$, and $T = 300$ K.

TABLE I. Lattice parameters of pristine α - V_2O_5 using DFT+ U and DFT+ U +vdW, and experimental values.

U (eV)	a (Å)	b (Å)	c (Å)	V (Å) ³
0	11.558	3.562	4.729	194.706
3	11.495	3.636	4.790	199.242
4	11.485	3.636	4.790	199.901
0+vdW	11.634	3.532	4.427	181.919
3+vdW	11.563	3.588	4.460	185.030
4+vdW	11.548	3.606	4.469	186.127
<i>Expt.</i> ^a	11.513	3.566	4.379	179.782
<i>Expt.</i> ^b	11.523	3.562	4.330	177.740

^aExperimental values were measured at 300 K, as reported in Ref. [13].

^bExperimental values were measured at 12 K, as reported in Ref. [14].

In Sec. III, we show and discuss the atomic structure and electronic properties of pure V_2O_5 as well as their changes in $Li_xV_2O_5$ ($x = 0.125$ and 0.25). We conclude our paper in Sec. IV.

II. COMPUTATIONAL DETAILS

A. DFT + U and structural optimization

We performed density functional theory (DFT)+ U calculations with a combination of the rotationally invariant formalism and the fully localized limit double-counting formula [35] implementing inside VASP package [36,37]. The projector augmented wave (PAW) method, which describes the relationship between core and valence electrons, was employed with the generalized gradient approximation (GGA) of Perdew-Burke-Ernzerhof (PBE) [38]. Since α - V_2O_5 exhibits a layered structure (Fig. 1), a van der Waals correction (vdW), specifically the DFT-D2 method [39,40], was also applied to relax the structure. For pristine and Li-doped V_2O_5 , we adopted $1 \times 2 \times 1$ and $1 \times 2 \times 2$ supercells, which correspond to V_8O_{20} and $V_{16}O_{40}$, respectively. The Hubbard U parameter varied from 0 to 6 eV, while Hund's coupling was fixed at $J = 0$ eV. We utilized the kinetic energy cutoff of 600 eV, and $3 \times 9 \times 4$ and $3 \times 5 \times 3$ k -point meshes for

TABLE II. Lattice parameters of $Li_{0.125}V_2O_5$ and $Li_{0.25}V_2O_5$ using DFT+ U and DFT+ U +vdW, and experimental data. We relax the structures using $1 \times 2 \times 1$ and $1 \times 2 \times 2$ supercells, and the values for the $1 \times 1 \times 1$ unit cell are shown.

x	U (eV)	a (Å)	b (Å)	c (Å)	V (Å) ³
0.125	0	11.498	3.564	4.742	194.322
	4	11.545	3.635	4.632	194.387
	0+vdW	11.562	3.534	4.453	181.941
	4+vdW	11.565	3.604	4.444	185.227
	<i>Expt.</i> ^a	11.480	3.620	4.420	183.685
	<i>Expt.</i> ^b	11.450	3.575	4.488	183.711
0.25	0+vdW	11.521	3.538	4.444	181.12
	4+vdW	11.514	3.552	4.548	185.980
	<i>Expt.</i> ^a	11.430	3.620	4.465	184.747
	<i>Expt.</i> ^b	11.420	3.570	4.525	184.482

^aExperimental values are derived from Ref. [28].

^bExperimental values are derived from Ref. [41].

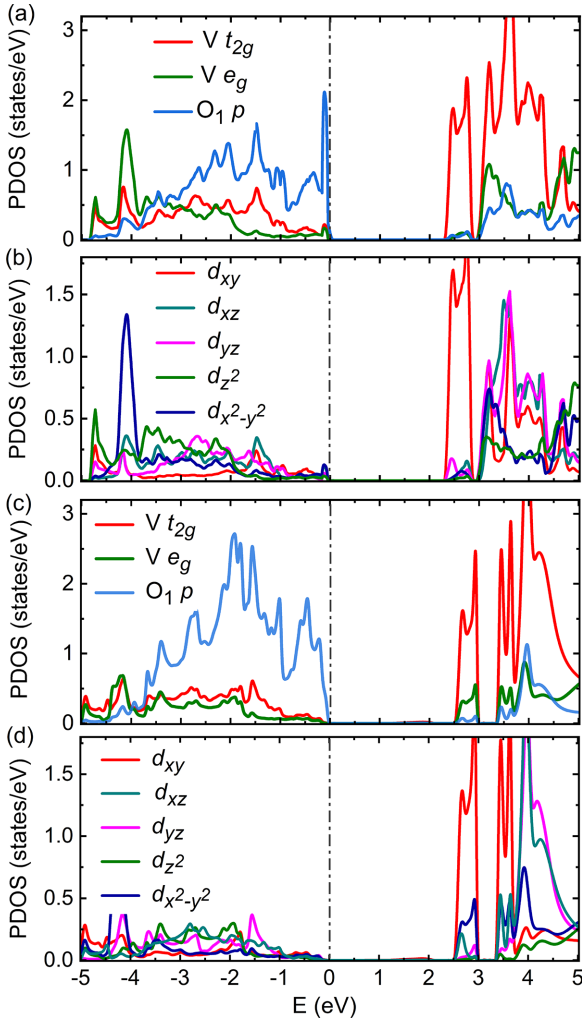


FIG. 3. Projected density of states onto V d and O p of pristine V_2O_5 , using (a),(b) DFT + U with $U = 4$ eV and $J = 0$ eV, and (c),(d) DFT + DMFT with $U = 5.5$ eV and $J = 0.5$ eV. $\lambda = 0.4$ and temperature $T = 300$ K are used. The valence-band maximum (VBM) is set to be zero.

$1 \times 2 \times 1$ and $1 \times 2 \times 2$ supercells, respectively. The convergence of the structural relaxation was achieved once the atomic forces of all ions reached a value less than 0.01 eV/Å.

We relaxed the lattice parameters of pristine α - V_2O_5 using different U values with and without vdW correction, as summarized in Table I. The intercalating distance between two layers increases (parameter c along the z -direction in Fig. 1) with increasing U . Without vdW correction, the c parameter increases from 4.729 to 4.790 Å with $U = 0$ – 4 eV. With vdW correction, the c parameter is suppressed from 4.427 to 4.469 Å with $U = 0$ – 4 eV. We conclude that DFT + U (=4 eV)+vdW gives the best lattice parameters compared to the experimental value $c = 4.392$ Å.

The lattice parameters of $Li_{0.125}V_2O_5$ and $Li_{0.25}V_2O_5$ are listed in Table II. The intercalating distance between two layers increases from 4.444 to 4.548 Å for $x = 0.125$ and 0.25 , respectively. Similar to the pristine case, the DFT + U + vdW with $U = 4$ eV gives the best match with the experiments. Since $U = 4$ eV also provides a reasonable band gap for the pristine α - V_2O_5 (Figs. 3 and 4), hereafter we focus on the

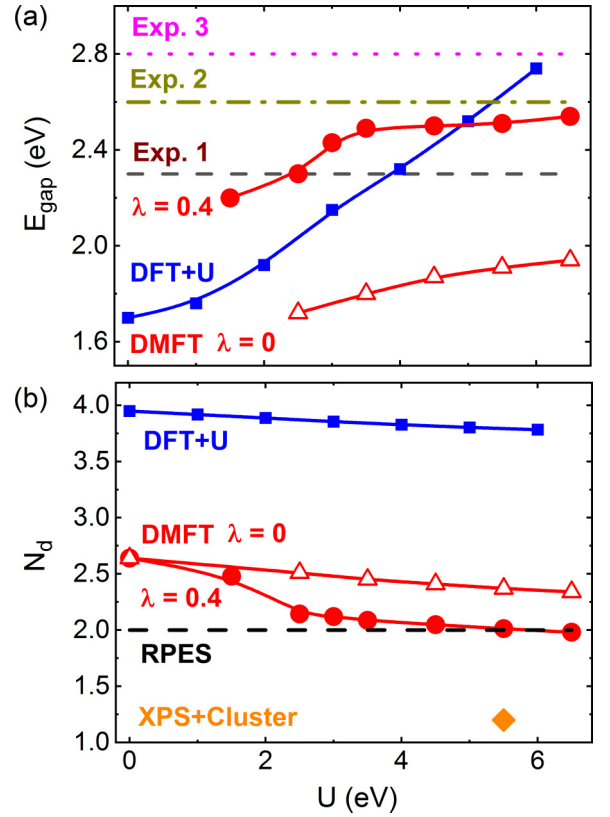


FIG. 4. (a) Energy gap (E_{gap}) of pristine V_2O_5 as a function of U . The experimental values of the band gap are taken from Ref. [18] (Exp. 1, black dashed line), Ref. [19] (Exp. 2, dark yellow dashed-dotted line), and Ref. [7] (Exp. 3, magenta dotted line). (b) The number of d electrons (N_d) of the V atom in V_2O_5 , as a function of U . Data of RPES and the cluster model are from Refs. [21] and [22], respectively. $J = 0$ is used for DFT + U , and $J = 0.5$ eV and $T = 300$ K are used for DMFT calculations. Two different values of the double counting parameter are shown: $\lambda = 0$ and 0.4 .

structure obtained using $U = 4$ eV within DFT + U + vdW, unless specified otherwise.

B. DFT + DMFT method

At the first step of a conventional DFT + DMFT procedure [41–43], we employ DFT + U + vdW to optimize atomic structures and subsequently create localized Wannier orbitals. For pristine V_2O_5 , we use $U = 4$ eV, as mentioned previously. On the other hand, in Li-doped V_2O_5 , the addition of electrons to the system leads to the emergence of two types of polarons [31,32], which result in distinct local structural distortions. However, the optimized structure obtained using $U = 4$ eV only provides the free polaron, where the electron is localized at a single V site, and significant structural relaxation is confined in the vicinity of this electron-localized V site. Therefore, to capture the structural distortion induced by the delocalized (or bound) polaron, we also relax the structure with $U = 0$ eV while maintaining fixed lattice parameters. By examining these two different structures, we can compare the two types of polarons within both DFT + U and DFT + DMFT. Further details can be found in Appendix C.

In the second step of DFT + DMFT calculations, V d and O p orbitals were constructed to represent a hybridization

subspace by projecting the Kohn-Sham (KS) plane-wave functions onto maximally localized Wannier functions (MLWFs) [44]. In this step, the non-spin-polarized DFT ($U = 0$ eV) scheme is used. In the last step, V d manifolds were implemented by using the continuous-time quantum Monte Carlo (CTQMC) impurity solver within DMFT [41,45,46]. An additional unitary rotation transformation for the Wannier subspace of V d orbitals was applied to minimize the off-diagonal hopping terms [41]. In these systems, we consider the hybridized region within an energy window of 10 eV around the Fermi level (see Fig. 10 in Appendix A).

The rotationally invariant Coulomb interaction in the form of the Slater-Kanamori interaction Hamiltonian [47–49] is

$$\hat{H}_{\text{SK}} = U \sum_{\alpha} \hat{n}_{\alpha\uparrow} \hat{n}_{\alpha\downarrow} + \frac{1}{2} \sum_{\alpha \neq \beta} \sum_{\sigma \sigma'} (U' - J \delta_{\sigma \sigma'}) \hat{n}_{\alpha\sigma} \hat{n}_{\beta\sigma'} - \sum_{\alpha \neq \beta} (J c_{\alpha\uparrow}^{\dagger} c_{\alpha\downarrow} c_{\beta\downarrow}^{\dagger} c_{\beta\uparrow} + J' c_{\beta\uparrow}^{\dagger} c_{\beta\downarrow} c_{\alpha\downarrow}^{\dagger} c_{\alpha\uparrow}). \quad (1)$$

Here, c_{σ} and c_{σ}^{\dagger} denote the fermion annihilation and creation operators, where σ is the spin. U denotes an intraorbital density-density interaction parameter, U' is an interorbital density-density interaction parameter, J is a spin-flip interaction parameter, and J' is a pair-hopping interaction parameter. $U' = U - 2J$ and $J' = J$ are due to rotational invariance.

To investigate the temperature effect, we employed electronic temperatures of 300 K. This choice is motivated by the application of V₂O₅ as a cathode material for batteries, which typically operate at room temperature. For single Li-doped V₂O₅, we also considered 150 K and found the electronic structures to be nearly indistinguishable. It is worth noting that within the CTQMC framework, we limited our considerations to density-density interactions. Given that there are 16 vanadium atoms in the supercell, a full Coulomb interaction calculation would be computationally demanding.

In the DMFT self-consistent calculations, the convergence of self-energy is determined once local or lattice self-energy $\Sigma^{\text{loc}}(i\omega_n)$ approaches the impurity self-energy $\Sigma^{\text{imp}}(i\omega_n)$, with the discrete Matsubara frequency ω_n [45,50]. [Note that the self-energy is approximated as a local quantity in the correlated subspace, i.e., $\Sigma(\mathbf{k}, i\omega_n) \simeq \Sigma(i\omega_n)$ [45].] So, the total DFT + DMFT energy is given by

$$E^{\text{TOT}} = E^{\text{DFT}}(\rho) + \sum_{m,\mathbf{k}} \epsilon_m(\mathbf{k}) \cdot [n_{mm}(\mathbf{k}) - f_m(\mathbf{k})] + E^{\text{POT}} - E^{\text{DC}}, \quad (2)$$

where E^{DFT} is the DFT energy computed by the electronic charge density ρ . $\epsilon_m(\mathbf{k})$ denotes the DFT eigenvalues, and $n_{mm}(\mathbf{k})$ and $f_m(\mathbf{k})$ are the diagonal DMFT occupancy matrix element and Fermi function, respectively, with the KS band m and momentum \mathbf{k} . The potential energy E^{POT} is calculated by using the Migdal-Galitski formula [51]:

$$E^{\text{POT}} = \frac{1}{2} \sum_{\omega_n} [\Sigma^{\text{loc}}(i\omega_n) G^{\text{loc}}(i\omega_n)]. \quad (3)$$

Here, the local Green's function is simplified by $G^{\text{loc}}(i\omega_n) = \sum_{\mathbf{k}} G^{\text{loc}}(\mathbf{k}, i\omega_n)$ [45,50].

Similar to the conventional fully localized limit, we used a double counting energy E^{DC} [42,43,50] to consider the double

counting corrections for the DFT + DMFT calculation as

$$E^{\text{DC}} = \frac{(U - \lambda)}{2} N_d(N_d - 1) - \frac{J}{4} N_d(N_d - 2), \quad (4)$$

where N_d is called the formal d -electron number obtained self-consistently at each V d site, and λ is the double counting parameter [43]. N_d is directly computed from the local Green function $G^{\text{loc}}(\mathbf{k}, \mathbf{k}', i\omega_n)$:

$$N_d = \sum_{a,n} \sum_{\mathbf{k}, \mathbf{k}'} \text{Im} \{ [\phi_d^a(\mathbf{k})]^* G^{\text{loc}}(\mathbf{k}, \mathbf{k}', i\omega_n) \phi_d^a(\mathbf{k}') \}. \quad (5)$$

Here, ω_n is the Matsubara frequency, and $\phi_d^a(\mathbf{k})$ represents the normalized d -orbital wave function, which is transformed from $\phi_d^a(\mathbf{r})$ with the real coordinates \mathbf{r} positioned on a transition-metal ion [52]. The spectral function or the density of states (DOS) is calculated by using the maximum entropy method [53]:

$$A(\omega_n) = -\frac{1}{\pi} \text{Im} \left[\sum_{\mathbf{k}} G^{\text{loc}}(\mathbf{k}, \omega_n) \right]. \quad (6)$$

III. RESULTS AND DISCUSSION

A. Pristine α -V₂O₅

As mentioned, α -V₂O₅ has a layered structure with a van der Waals interaction between the layers. A vanadium atom is located at a distorted pyramidal coordination surrounded by five oxygen atoms, which are classified into three different types, as depicted in Fig. 1: (i) vanadyl oxygen (O₁ forms a double bond with the vanadium atom), (ii) bridge oxygen (O₂ connects two vanadium atoms in different chain), and (iii) chain oxygen (O₃ bonds to three vanadium atoms) [3,54].

V has a 5+ charge state with d^0 in V₂O₅, and thus the conduction bands are largely dominated by V d bands, whereas the valence bands near the Fermi level are significantly from O p bands (Figs. 2 and 3). From the structure of V-O bonds, V $d_{x^2-y^2}$ and d_{z^2} form σ bonds and p orbitals of O₁ and O₂ + O₃ atoms, respectively, while t_{2g} orbitals form π bonds with O atoms. Since one of the apical oxygens is missing compared to the VO₆ octahedron, the cubic symmetry of d bands is broken. Thus, doubly degenerate e_g bands split into $d_{x^2-y^2}$ and d_{z^2} bands, and t_{2g} bands break into d_{xy} bands as well as double degeneracy of $d_{xz} + d_{yz}$ bands, as presented in Fig. 3. As a result, there is splitting in the V d states in the conduction band, as presented in Fig. 3. The lower band is called the ‘‘split-off band,’’ and the higher band is named the ‘‘main conduction band.’’

We first study the effect of U on the width of the energy gap (E_{gap}) and the CB gap (due to separating between the split-off band and the main conduction band) using DFT + U , as illustrated in Fig. 4(a). At $U = 0$ eV, $E_{\text{gap}} = 1.7$ eV is much smaller than the experimental values of 2.3 – 2.8 eV [7,18,19]. The CB gap of 0.4 eV is comparable to the experimental splitting 0.5 eV [6,55]. At $U = 4$ eV, $E_{\text{gap}} = 2.3$ eV agrees well with prior DFT + U studies [13,22] and the experiments. However, the CB gap is only 0.20 eV, which is narrower than the experimental result [6,55]. Therefore, we remark that E_{gap} ascends with respect to U , whereas the CB splitting width descends versus U .

In Fig. 4(b), we observe that DFT + U overestimates the number of d electron (N_d) in V. This value is around 3.8 – 4.0

TABLE III. Contribution of $3d^n L^n$ states to the ground state of V_2O_5 .

Configuration	DMFT	Cluster [22]
$3d^0$	2%	20%
$3d^1 L$	22%	47%
$3d^2 L^2$	41%	28%
$3d^3 L^3$	25%	N/A

in the U range of 0 – 6 eV, but larger than the experimental ones such as $N_d = 2.0$ measured by RPES [21], and 1.2 calculated by the cluster model based on XPS and XAS [22]. Therefore, DFT + U has a critical limitation to describe the physics of V d bands. We also note that the N_d value depends on the projection methods. At $U = 0$ eV, N_d using the Wannier projectors gets 2.64 [corresponding to DMFT with $U = 0$ in Fig. 4(b)], and it is smaller than $N_d = 4.0$ from the PAW projectors.

To resolve the limitation of DFT + U , we performed DFT + DMFT calculations for pristine α - V_2O_5 . First, we compute E_{gap} as a function of U without the double counting parameter (i.e., $\lambda = 0$) [Fig. 4(a)]. At $\lambda = 0$, E_{gap} is 1.71–1.95 eV with $U = 2.5$ –6.5 eV and less sensitive on U in comparison with DFT + U , and it does not approach the experimental value of 2.3–2.8 eV [7,18,19]. Since V_2O_5 is shown to be a charge-transfer insulating system, the p - d hybridization is more important than the d - d correlation for determining its band gap. The double counting correction λ controls the degree of p - d covalency, and increasing this parameter results in a larger separation between O p and V d bands and thus it enlarges E_{gap} . At $\lambda = 0.4$, we obtain $E_{\text{gap}} = 2.35$ –2.55 eV for U values of 2.0–6.5 eV, which are in very good agreement with the experimental values.

Nonzero λ is also needed for a reasonable N_d , as depicted in Fig. 4(b). The N_d values using $\lambda = 0$ with $U = 1.5$ – 6.5 eV are 2.50 – 2.34, always larger than the experimental values [21,22,56]. If $\lambda = 0.4$ is implemented, we show $N_d = 2.50$ – 1.98 with the range of U from 2.5 to 6.5 eV. In particular, $N_d = 2.01$ for $U = 5.5$ eV matches well with the RPES value [21]. Therefore, combining the results of E_{gap} and N_d , we conclude that $U = 5.5$ eV and $\lambda = 0.4$ are the best parameters for DMFT computations, with $E_{\text{gap}} = 2.52$ eV and $N_d = 2.01$.

Different from our DMFT calculation and the previous RPES measurement ($N_d = 2.0$) [21], Mossaneck *et al.* showed $N_d \sim 1.2$ from the single impurity cluster model, solved by the configuration interaction method [22]. They considered $[\text{VO}_5]^{-5}$ (V^{5+}) with C_{4v} symmetry, corresponding to the square base pyramid structure. To explain the difference of N_d between our DMFT and the cluster model, we calculate the contribution of $d^n L^n$ configurations to the ground state of α - V_2O_5 , as summarized in Table III. The weight of d^0 is only 2% within DMFT, whereas it is 20% from the cluster model [22]. From our DMFT calculations, the $3d^2 L^2$ configuration has the largest weight of 41%, and $3d^1 L^1$ and $3d^3 L^3$ account for 22% and 25% of population probabilities, respectively. Within the cluster model, $3d^1 L^1$ contributes the largest probability of 47%, and the weight of the $3d^2 L^2$ configuration is

28% [22]. We note that the single impurity cluster model does not include the hybridization between clusters, i.e., there are no V-V or O-O interactions, and therefore both the d and p states do not have dispersion. The absence of the band dispersion in their model may give rise to the suppression of N_d .

Spectral functions, i.e., DOS from DMFT calculations using $U = 5.5$ eV and $\lambda = 0.4$, are presented in Figs. 3(c) and 3(d). The CB gap of 0.4 eV between the split-off band and the main conduction band is close to the experimental value 0.5 eV from the photoluminescence measurements [6,55]. We emphasize that while DFT + U only provides a reasonable value of E_{gap} , experimental values of E_{gap} , N_d , and CB gap are successfully reproduced by our DMFT calculations. That implies that an accurate method for electron correlation is essential, even for d^0 band systems. Similar to DFT + U , the split-off band is mainly from the d_{xy} band within DMFT. The O p character is dominant near the valence-band maximum, especially between -3.5 and -2.0 eV [Fig. 3(c)]. In Fig. 2, we also show that our DMFT DOS are well matched to UPS [57] and HAXPES [12] experiments, particularly at the positions of the Fermi level and the range of valence band.

B. α -Li $_x$ V $_2$ O $_5$ ($x = 0.125$ and 0.25)

In this section, we consider Li-doped α - V_2O_5 , including α -Li $_{0.125}$ V $_2$ O $_5$ and α -Li $_{0.25}$ V $_2$ O $_5$, using both DFT + U and DMFT methods.

1. α -Li $_{0.125}$ V $_2$ O $_5$

α -Li $_{0.125}$ V $_2$ O $_5$ is formed by intercalating one Li atom in the $1 \times 2 \times 2$ supercell (corresponding to Li $_1$ V $_{16}$ O $_{40}$). The distance between Li ions in the next supercell is 11.55, 7.21, and 8.94 Å along the a , b , and c directions, respectively. Thus, we assume that the interaction between Li defects is almost negligible once the periodic boundary condition is implemented. We examined several different initial positions of a doping single Li ion (see Appendix B), and we found that the most stable position of the Li ion is the middle of a hole, as depicted in Fig. 5(a). The Li atom gets closer to the lower layer than the upper layer [Fig. 5(b)]. Distances from the Li ion to the lower and upper V layers are 3.506 and 5.381 Å, respectively. The stable position of the Li ion is similar to the structure obtained in the previous DFT + U studies [12,23].

Once Li atoms are doped, they donate one electron per Li ion to the V_2O_5 system and become Li $^+$. Li s bands are fully empty and far above the Fermi level by 6.5 eV, indicating Li $^+$. Within DFT + U , the splitting between the split-off band and the main CB becomes even smaller for Li $_{0.125}$ V $_2$ O $_5$, and the CB gap is nearly zero, while the CB gap is 0.1 eV for pristine α - V_2O_5 within DFT + U (Fig. 6).

DFT + U results show that a defect level is created at the middle of the band gap for doping a single Li-ion in the V_2O_5 framework [Figs. 6(a)–6(b)]. The defect band occupies one electron, the spin-up defect level is filled and located 0.62 eV above the VBM, while the spin-down level is empty. The position of the spin-up defect level is similar to the previous DFT + U ($=4$ eV) study of α -Li $_{0.028}$ V $_2$ O $_5$ (corresponding to Li $_1$ V $_{72}$ O $_{180}$), where the Li defect level is near VBM + 1.0 eV [23].

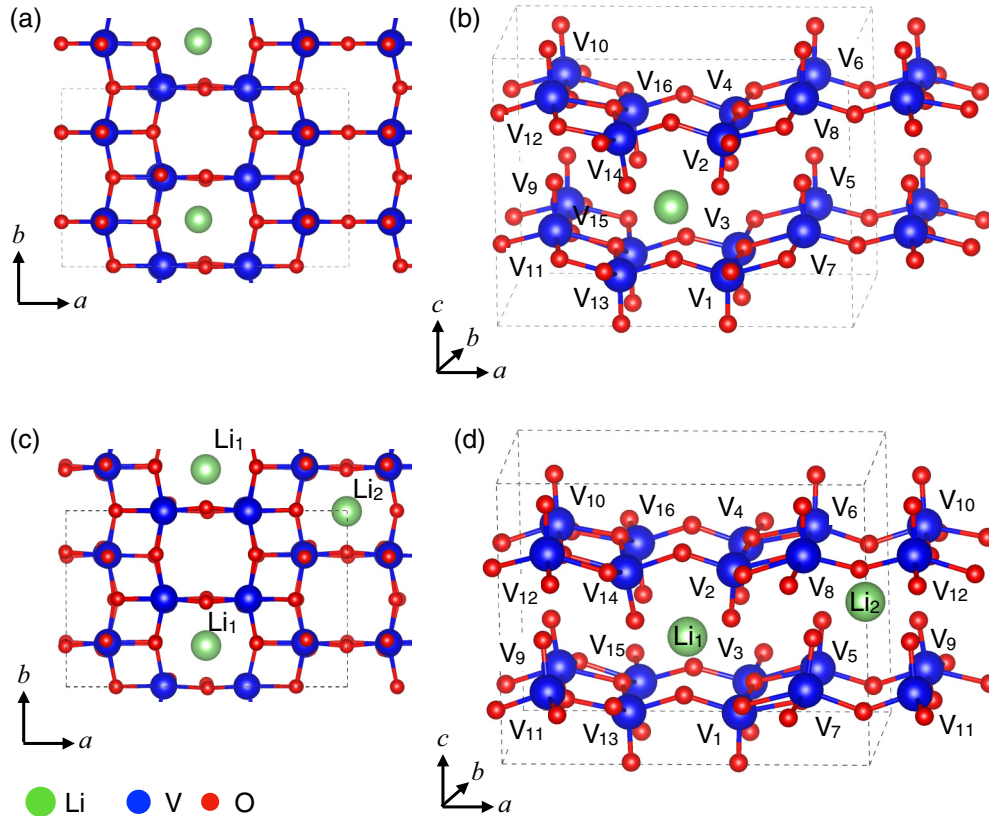


FIG. 5. Atomic structure of (a),(b) $\text{Li}_{0.125}\text{V}_2\text{O}_5$ and (c),(d) $\text{Li}_{0.25}\text{V}_2\text{O}_5$. Indices of V atoms are shown.

The origin of the defect level is the charge disproportionation of the V atoms, since the electron occupying the defect level is spatially localized on a single V atom (see Fig. 7). Given that only the spin-up defect band is occupied, the magnetic moments of V atoms shown in Table IV directly indicate the charge disproportionation in Li-doped V_2O_5 within DFT + U . Specifically, one electron from Li is donated at the V_{15} atom, which is the nearest neighbor of the Li atom with a distance of 3.075 Å (see Fig. 5).

The localization of the electron induces a polaronic effect in $\text{Li}_x\text{V}_2\text{O}_5$ [12,31,32,58]. The ESR and ENDOR spectroscopies and the electronic conductivity measurement proposed two types of charge carriers in $\text{Li}_{0.005}\text{V}_2\text{O}_5$ [32] and $\text{Li}_{0.001}\text{V}_2\text{O}_5$ [31]: (i) free polarons localized at single vanadium sites, and (ii) bound polarons delocalized over four vanadium sites around a Li^+ ion (see Fig. 8 for schematic illustrations). Since the electron prefers to occupy a single V, this corresponds to the free polaron [Fig. 8(a)]. According to previous DFT + U studies, the electron could be positioned on other V sites with a higher value than the ground state by 0.1–0.2 eV [33]. The migration barrier from DFT + U calculations is 0.12–0.34 eV [33,34], close to the experimental values 0.27–0.28 eV [58,59]. However, the bound polaron has not been observed by DFT + U calculations.

To explore the polaronic effect suggested in the previous experiments [31,32], we performed DFT + DMFT calculations using parameters analogous to those of pristine V_2O_5 ($U = 5.5$ eV, $J = 0.5$ eV, and $\lambda = 0.4$ at $T = 300$ K). We

examined two different types of structural distortions, as stated in Sec. II B. By considering two different structures, we aim to disentangle the effect of structural distortion and electron correlation on the electron distribution. Surprisingly, as shown in Table V, the bound polaron is more stable than the free polaron within DMFT, while the energy difference is only 0.11 eV. We emphasize that the experiments observed simultaneously both types of polarons [31,32,58], which are fruitfully interpreted by a smaller energy difference between the two states within our DFT + DMFT results (Table V). Furthermore, both states can also explain the diminishing effect of d_{xy} (or d_{xy} occupation) and inhomogeneous electron distribution by scanning transmission x-ray microscopy (STXM) in Li-doped V_2O_5 [12,25].

For the free polaron within DFT + DMFT, the doped electron predominantly occupies the V_{15} site, similar to DFT + U . The electron gain of V_{15} is $0.46e$, while N_d for V_2 , V_4 , V_{14} , and V_{16} exhibit a slight increase, ranging from $0.05e$ to $0.08e$ [see Fig. 7(a)]. The bound polaron depicted by DFT + DMFT is notably intriguing. This state has no defect level in the band gap and is hidden above the CBM [Figs. 9(a)–9(c)]. The electron at the Li defect level is thus empty, and doped electrons are occupying the V d_{xy} state of the split-off band. V ions at the lower layer (V_1 , V_3 , V_{13} , and V_{15}) gain the largest number of electrons at around $0.12e - 0.16e$ per V atom [Fig. 9(a)], while the upper-layer V ions (V_2 , V_4 , V_{14} , and V_{16}) also increase by about $0.05e$ [Fig. 9(b)]. On the other hand, the other V ions far from the Li ion lose $0.03e$ per V

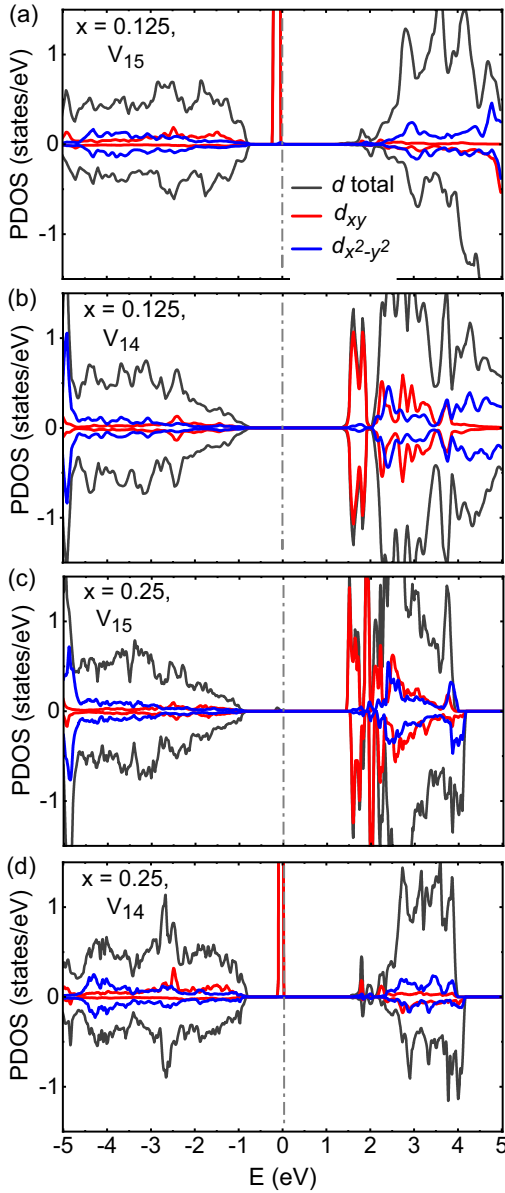


FIG. 6. DOS and projected density of states (PDOS) onto a V d orbital for (a),(b) α - $\text{Li}_{0.125}\text{V}_2\text{O}_5$ and (c),(d) α - $\text{Li}_{0.25}\text{V}_2\text{O}_5$, using DFT + U . $U = 4$ eV and $J = 0$ eV are used. Fermi energy is set to zero.

atom, and their d bands are empty [Fig. 9(c)]. Our DMFT result indicates that the electron localizes in V ions close to the Li site, consistent with experiments [31,32].

To understand the reason why we cannot observe the bound polaron by DFT + U with full atomic relaxation, we carried out a simple test by taking the bound polaron structure within DMFT calculation and then adopting the spin-polarized DFT + U ($=4$ eV) + vdW. As presented in Table V, the total energy of the bound polaron is higher than the free one by 0.51 eV, indicating that the bound polaron is unstable within DFT + U . Our results suggest that electron localization in V_2O_5 is overestimated within DFT + U , and the discrepancy is rectified by DFT + DMFT.

Another important feature from our DMFT results is the nonzero CB gap of 0.4 eV for $\text{Li}_{0.125}\text{V}_2\text{O}_5$, as depicted in

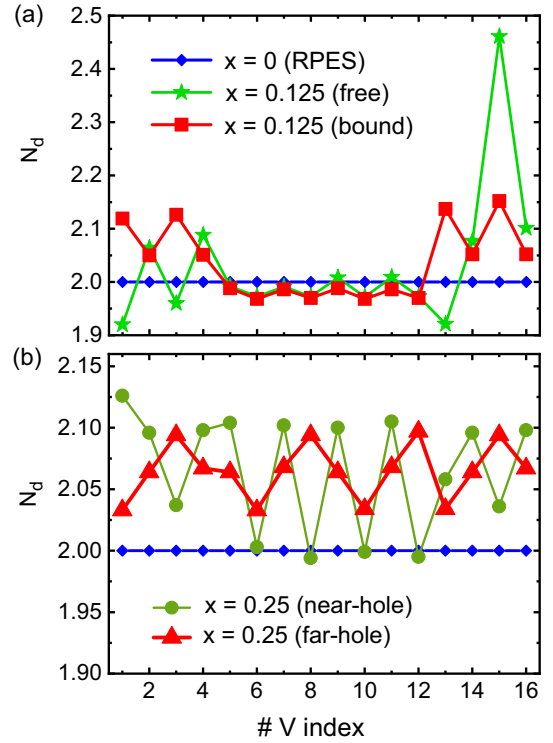


FIG. 7. N_d of V atoms in $\text{Li}_x\text{V}_2\text{O}_5$ for (a) $x = 0.125$ and (b) $x = 0.25$. The N_d value is calculated by the DFT + DMFT method with $U = 5.5$ eV, $J = 0.5$ eV, and $\lambda = 0.4$ at $T = 300$ K. We consider the Li^+ ion as the center of system, and we classify the N_d values into a high value for the nearest V atom, a medium value for the next-nearest V atom, and a low value for far V atoms (see Fig. 5). The blue diamond with a line shows the background homogeneous N_d of the V atom in our pristine V_2O_5 and RPES measurement [21]. The V atoms that have $N_d > 2.0$ will receive an electron donated by the Li atom.

Figs. 9(a)–9(c). Recent photoluminescence, optical absorption, and photoemission spectroscopy suggested that the CB gap is 0.5 eV for $\text{Li}_x\text{V}_2\text{O}_5$ ($0 \leq x \leq 1$) [6]. Therefore, while DFT + U fails to obtain a nonzero CB gap for Li-doped V_2O_5 , the splitting of the split-off band and the main CB gap is successfully described by DMFT.

2. α - $\text{Li}_{0.25}\text{V}_2\text{O}_5$

We now consider $\text{Li}_{0.25}\text{V}_2\text{O}_5$ by adding two Li atoms in the $1 \times 2 \times 2$ supercell (the stoichiometric formula is $\text{Li}_2\text{V}_{16}\text{O}_{40}$). From the experiment, α and ϵ phases coexistent for $x = 0.25$ [27–29], but we only consider α - $\text{Li}_{0.25}\text{V}_2\text{O}_5$. As shown in Fig. 5, we choose two Li ions positioned at two of the four large holes: (i) *near-hole* with an Li-Li distance ($d_{\text{Li-Li}}$) of

TABLE IV. Magnetic moments (μ_B) of V atoms in α - $\text{Li}_x\text{V}_2\text{O}_5$ ($x = 0.125$ and 0.25), within DFT + U calculations. $U = 4$ eV and $J = 0$ are used. Indices of V atoms are shown in Fig. 5.

$x =$	V ₁	V ₂	V ₃	V ₇	V ₁₁	V ₁₃	V ₁₄	V ₁₅	other V
0.125	0.01	0.00	0.08	0.00	0.00	0.01	0.02	1.11	0.00
0.25	0.00	0.13	0.00	1.08	0.12	0.00	1.08	0.00	0.00

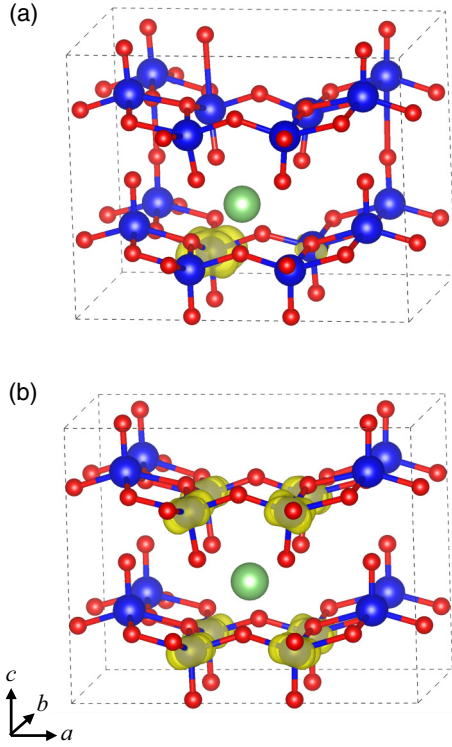


FIG. 8. Schematic illustration of (a) free and (b) bound polarons in $\text{Li}_{0.125}\text{V}_2\text{O}_5$. The atomic positions are referred to in Fig. 5(b).

3.166 Å, and (ii) *far-hole* with $d_{\text{Li-Li}} = 8.104$ Å. The far-hole configuration is more stable than the near-hole structure by 0.19 eV because the Coulomb interaction between Li^+ ions becomes weaker. Hereafter we only focus on the far-hole configuration.

The electronic properties of the $x = 0.25$ case behave relatively similar to those of the $x = 0.125$ case. Within DFT + U , the electron or free polaron is strongly localized at the defect level, i.e., two doped electrons are trapped on V_7 and V_{14} [see Table IV and Figs. 6(c) and 6(d)]. Therefore, the spin-up defect levels are almost degenerate near 0.62 eV above the VBM [Fig. 6(c)].

The bound polaronic state in $x = 0.25$ by DFT + DMFT shows that the electron is more delocalized than $x = 0.125$. As presented in Figs. 7(b) and 9(d)–9(f), d bands of all V atoms gain electrons and partially occupy, so the distribution of doped electrons in $\text{Li}_{0.25}\text{V}_2\text{O}_5$ becomes more homogeneous than in $\text{Li}_{0.125}\text{V}_2\text{O}_5$. The defect level occurs in the band gap,

TABLE V. Energy difference between free and bound polarons calculated within DFT + U and DMFT for $\text{Li}_{0.125}\text{V}_2\text{O}_5$. Here, we used spin-polarized DFT + U with $U = 4$ eV and $J = 0$ eV. The parameters for DMFT are $U = 5.5$ eV and $J = 0.5$ eV, $\lambda = 0.4$ at room temperature. We set the energy level of the free polaron at 0 eV and compare with the bound one.

Methods	Free polaron	Bound polaron
DFT+ U	0	0.51 eV
DMFT	0	-0.11 eV

and electrons are occupied V d_{xy} bands, which results in the metallic state compared with the prediction of the insulating case by DFT + U .

When x is increased from 0.125 to 0.25, the Fermi level within DMFT is increased since the additional electrons are occupying the lowest conduction band (d_{xy}), while the electrons are occupying the midgap defect state and thus the Fermi level is unchanged within DFT + U . As shown in Figs. 4 and 9, the Fermi level from DMFT with respect to the valence-band maximum (VBM) is increased from 2.52 to 2.83 eV for $x = 0$ to 0.25. Indeed, the photoluminescence, optical absorption, and depth-resolved cathodoluminescence spectroscopies suggested the occurrence of the Burstein-Moss effect in Li-doped V_2O_5 [6,25,30], consistent with our DMFT results.

IV. CONCLUSION

Based on the DFT + U and DFT + DMFT study, we have shown that a precise description of the electron correlation is important in the electronic structure of V_2O_5 and $\text{Li}_x\text{V}_2\text{O}_5$ ($x = 0.125$ and 0.25). For pristine V_2O_5 , we compare three experimental quantities: (i) the band gap ($E_{\text{gap}} = 2.6$ eV), (ii) the gap in the conduction band (CB gap = 0.4 – 0.5 eV), and (iii) the number of d electrons of V ($N_d = 2.0$). While both the experimental band gap and the CB gap can be obtained using DFT + U , N_d is twice as large as the experimental value, indicating that the O p -V d hybridization is overestimated by DFT + U .

Our DMFT results shows that for the zero double counting correction, the band gap is not very sensitive for U , and it is much smaller than the experimental value even with $U = 6.5$ eV. We found that using a nonzero double counting term enlarges the band gap and provides an experimental value. Since the nonzero double counting term suppresses the p - d hybridization, it is important in the band gap of the charge-transfer insulator V_2O_5 .

The difference between DFT + U and DMFT results is more dramatic for Li-doped V_2O_5 . For both $\text{Li}_{0.125}\text{V}_2\text{O}_5$ and $\text{Li}_{0.25}\text{V}_2\text{O}_5$ using the DFT + U method, only the free polaron is preferable, i.e., defect levels are formed in the middle of the band gap. The spin-up defect levels are fully occupied by electrons from Li, and the conduction band is empty. Spatially, the electron at the defect level is localized on one vanadium site. Our DMFT results show both types of polarons as ESP and ENDOR suggested [31,32], and the delocalized polaronic state is energetically more stable than the free one. In this state, the doped electrons are localized mostly over four vanadium sites. Thus, the defect level is empty and hidden in the conduction band, and the electron is occupying at the split-off band, resulting in the increase of the conduction band. The Fermi level shift with Li doping is consistent with the recently observed Burstein-Moss shift, in which absorption energy shifts to higher energies from the optical absorption and photoemission spectroscopy [6,25].

ACKNOWLEDGMENTS

This work was supported by U.S. Department of Energy under Contract DE-AC02-06CH11357 from the Vehicle

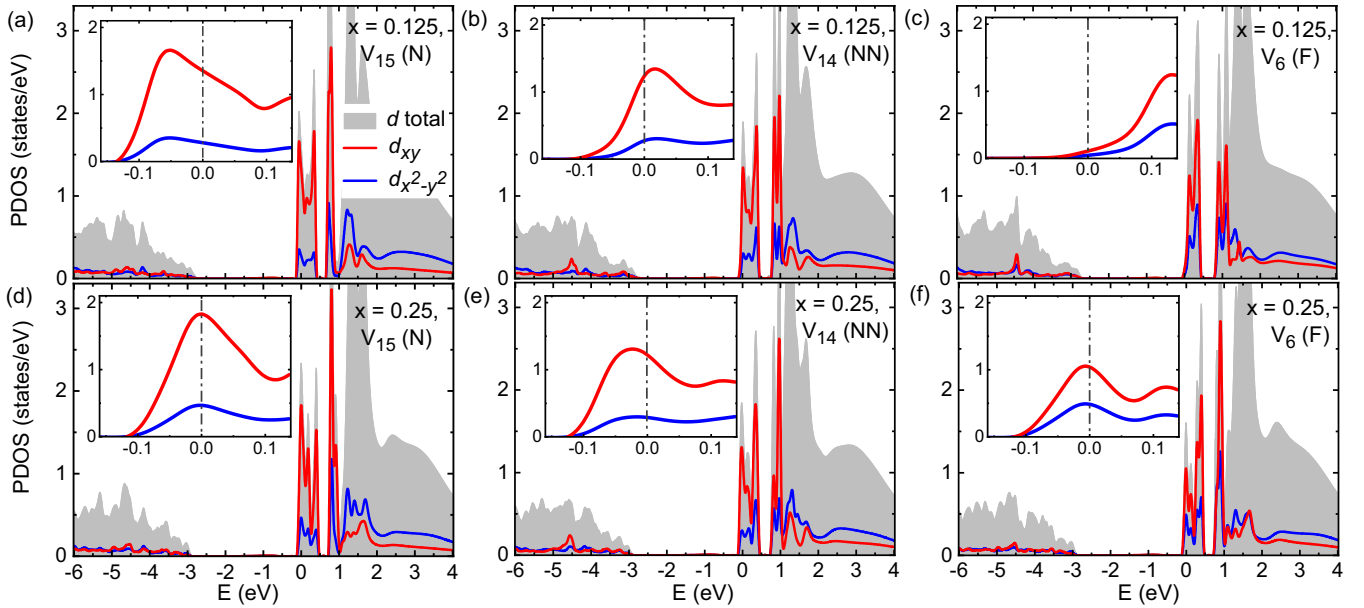


FIG. 9. Projected density of states (PDOS) onto the V d orbital within DMFT, for (a)–(c) α -Li_{0.125}V₂O₅, and (d)–(f) α -Li_{0.25}V₂O₅. We choose V sites which are nearest neighbors (N) of Li (V₁₅), next nearest neighbors (NN) of Li (V₁₄), and far (F) from Li ions (V₆). Here, we use $U = 5.5$ eV, $J = 0.5$ eV, $\lambda = 0.4$, and temperature $T = 300$ K. The Fermi level is set to be zero, and the insets zoom in the region near the Fermi level. This figures show the bound polaronic effects in Li-doped V₂O₅.

Technologies Office, Office of Energy Efficiency and Renewable Energy. We also acknowledge financial support from the U.S. Department of Energy, Office of Science, Office of Basic Energy Sciences, Materials Science and Engineering Division. We gratefully acknowledge the computing resources provided on Bebop, a high-performance computing cluster operated by the Laboratory Computing Resource Center at Argonne National Laboratory.

APPENDIX A: BAND STRUCTURE OF PRISTINE α -V₂O₅

In Fig. 10, we compare the DFT and Wannier band structures. The result indicates that the plane-wave functions fit very well with the localized orbital functions.

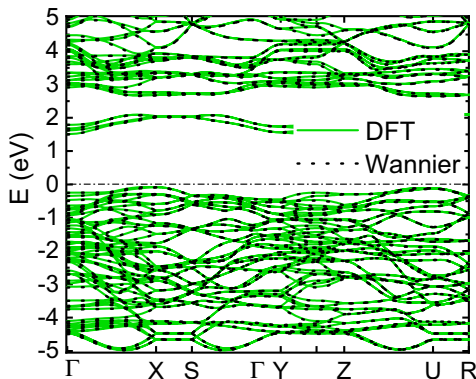


FIG. 10. Band structure calculated by DFT and Wannier function for pristine α -V₂O₅. Fermi level is set at zero.

APPENDIX B: OPTIMIZING THE LI ATOM POSITION IN THE V₂O₅ SYSTEM

In this Appendix, we present our relaxations of Li _{x} V₂O₅ ($x = 0.125$ and 0.25) systems. Several positions of Li atoms in the V₂O₅ framework were checked carefully. With $x = 0.125$, a single Li atom was inserted in a $1 \times 2 \times 2$ supercell (stoichiometric formula of Li₁V₁₆O₄₀) (see Table VI). First, we inserted a random position of the Li atom [as shown in Fig. 11(a)], and after the relaxing process, it moved and located at the middle of the “hole,” which is surrounded by four vanadium atoms (front view). Second, in order to confirm that the middle of the hole is the most stable position, we adjusted the Li⁺ ion around it. We note that the position of the Li⁺ ion in the off-center gave us a little lower energy of 20 meV than the center. Also, when comparing with the previous DFT + U results about Li-inserted V₂O₅ [12,23], we conclude that the most stable location for the Li⁺ ion is the middle of the hole (see Fig. 12).

Since the middle of the hole is the most stable location for the Li⁺ ion, with $x = 0.25$, there are four holes in the supercell. So, we placed the first Li₁⁺ ion in the hole, which is similar to the $x = 0.125$ case, and then we chose the second one in the near or far hole (Fig. 13). As shown in Table VII, we observe that the far-hole situation has lower energy than

TABLE VI. Different configuration of Li⁺ ion in supercell 122 using DFT + U , $U = 4$ eV, and $J = 0.0$ eV.

Config.	Change E (eV)	Mom. (μ_B)
Center	0.02	1
Off-center	0	1

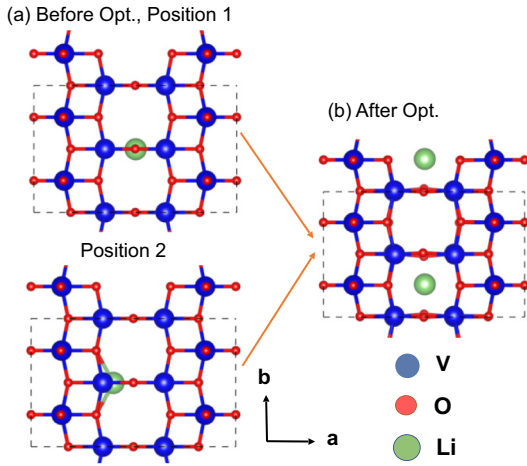


FIG. 11. Atomic structure of $\text{Li}_{0.125}\text{V}_2\text{O}_5$ (a) before and (b) after optimizations.

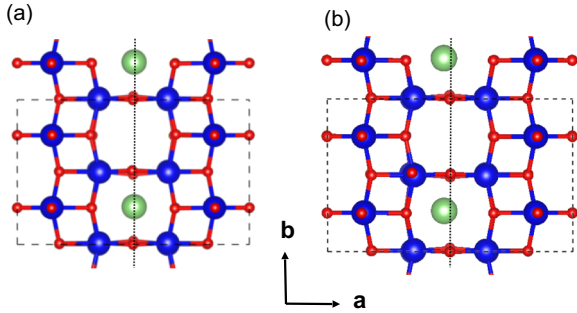


FIG. 12. Atomic structure of $\text{Li}_{0.125}\text{V}_2\text{O}_5$ for (a) Li^+ ion at the center of the hole and (b) Li^+ ion at the off-center of the hole.

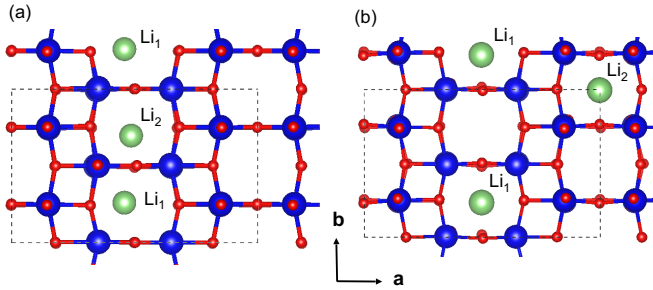


FIG. 13. Atomic structure of $\text{Li}_{0.25}\text{V}_2\text{O}_5$ for (a) near-hole and (b) far-hole.

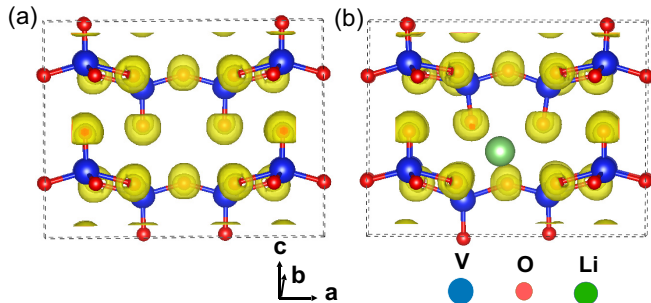


FIG. 14. Isosurface plots of the electron localization function for (a) V_2O_5 and (b) $\text{Li}_{0.125}\text{V}_2\text{O}_5$.

TABLE VII. Relative energies of the two different atomic configurations for $\text{Li}_{0.25}\text{V}_2\text{O}_5$, with different spin order. Here we used DFT + U with $U = 4$ eV and $J = 0$ eV.

Config.	Energy (eV)	Mag. mom. (μ_B)
Near-hole	0.19	2 (FM)
Near-hole	0.19	0 (AFM)
Far-hole	0	2 (FM)

the near-hole one by 190 meV by minimizing the Coulomb interaction between two Li^+ ions in the system. We took the far-hole structure for further DMFT study.

APPENDIX C: TESTING THE FREE AND BOUND POLARONS IN $\text{Li}_{0.125}\text{V}_2\text{O}_5$ USING DFT + U AND DMFT METHODS

1. Free polaron

We used DFT + U ($= 4$ eV) + vdW to optimize the atomic structure. From the optimal structure, we solve the non-spin-polarized Kohn-Sham equation using DFT + U ($= 0$ eV) + vdW within VASP. Then, we performed the localized orbital interpolation. Finally, we applied the correlation and hybridization effects to the system within DMFT. By that way, the free polaron was observed by DFT + DMFT. This is a standard procedure for DFT + DMFT calculation, and it is described in Refs. [41,43].

2. Bound polaron

There are two reasons why we want to observe the atomic scale existence of the bound polaron. First, experimental measurements, including ESR, ENDOR, and electronic conductivity, suggested the coexistence of free and bound polarons in $\alpha\text{-Li}_x\text{V}_2\text{O}_5$. Second, none of the DFT + U works have predicted these polaron. However, we have seen that at DFT + U ($= 0$ eV), the doped electron is more delocalizing in the system. So, we altered the standard DFT + DMFT computation as follows: (i) From the DFT + U ($= 4$ eV) + vdW structure, we reoptimized it with $U = 0$ eV with a fixed lattice parameter and non-spin-polarized schemes inside VASP. (ii) We took this structure for additional steps, such as Wannierization and self-consistent DMFT calculation. We also test the bound polaronic state in DFT + U by simply applying $U = 4$ eV on the optimal DFT, as shown in Table V.

APPENDIX D: ELECTRON LOCALIZATION FUNCTION

With the optimal structures of $\text{Li}_x\text{V}_2\text{O}_5$ ($x = 0$ and 0.125) obtaining in Sec. II A, we plot their electron localization function isosurfaces within DFT + U using $U = 4$ eV (as shown in Fig. 14). In the nature bond between V and O, we recognize that electrons are localized at O sites, which indicates ionic bonding [60–62].

- [1] P. Hu, P. Hu, T. D. Vu, M. Li, S. Wang, Y. Ke, X. Zeng, L. Mai, and Y. Long, Vanadium oxide: Phase diagrams, structures, synthesis, and applications, *Chem. Rev.* **123**, 4353 (2023).
- [2] P. Flowers, K. Theopold, and R. Langley, *Chemistry* (Open Stax, Houston, Texas, 2015).
- [3] O. Šipr, A. Šimůnek, S. Bocharov, T. Kirchner, and G. Dräger, Geometric and electronic structure effects in polarized V K-edge absorption near-edge structure spectra of V_2O_5 , *Phys. Rev. B* **60**, 14115 (1999).
- [4] S. Shin, S. Suga, M. Taniguchi, M. Fujisawa, H. Kanzaki, A. Fujimori, H. Daimon, Y. Ueda, K. Kosuge, and S. Kachi, Vacuum-ultraviolet reflectance and photoemission study of the metal-insulator phase transitions in VO_2 , V_6O_{13} , and V_2O_3 , *Phys. Rev. B* **41**, 4993 (1990).
- [5] G. A. Horrocks, E. J. Braham, Y. Liang, L. R. D. Jesus, J. Jude, J. M. Velázquez, D. Prendergast, and S. Banerjee, Vanadium K-edge X-ray absorption spectroscopy as a probe of the heterogeneous lithiation of V_2O_5 : First-principles modeling and principal component analysis, *J. Phys. Chem. C* **120**, 23922 (2016).
- [6] Q. Wang, M. Brier, S. Joshi, A. Puntambekar, and V. Chakrapani, Defect-induced Burstein-Moss shift in reduced V_2O_5 nanostructures, *Phys. Rev. B* **94**, 245305 (2016).
- [7] J. Meyer, K. Zilberberg, T. Riedl, and A. Kahn, Electronic structure of vanadium pentoxide: An efficient hole injector for organic electronic materials, *J. Appl. Phys.* **110**, 033710 (2011).
- [8] G. L. Simard, J. F. Steger, R. J. Arnott, and L. A. Siegel, Vanadium oxides as oxidation catalysts, *Ind. Eng. Chem.* **47**, 1424 (1955).
- [9] L. R. De Jesus, G. A. Horrocks, A. Parija, C. Jaye, L. Wangoh, J. Wang, D. A. Fischer, L. F. J. Piper, D. Prendergast, and S. Banerjee, Mapping polaronic states and lithiation gradients in individual V_2O_5 nanowires, *Nat. Commun.* **7**, 12022 (2016).
- [10] M. S. Whittingham, The role of ternary phases in cathode reactions, *J. Electrochem. Soc.* **123**, 315 (1976).
- [11] S. H. Lim, D. H. Kim, J. Y. Byun, B. K. Kim, and W. Y. Yoon, Electrochemical and catalytic properties of V_2O_5/Al_2O_3 in rechargeable LiO_2 batteries, *Electrochim. Acta* **107**, 681 (2013).
- [12] C. Ruan, X. Wang, C. Wang, L. Zheng, L. Li, J. Lin, X. Liu, F. Li, and X. Wang, Selective catalytic oxidation of ammonia to nitric oxide via chemical looping, *Nat. Commun.* **13**, 718 (2022).
- [13] M. B. Smirnov, E. M. Roginskii, K. S. Smirnov, R. Baddour-Hadjean, and J.-P. Pereira-Ramos, Unraveling the structure-raman spectra relationships in V_2O_5 polymorphs via a comprehensive experimental and DFT study, *Inorg. Chem.* **57**, 9190 (2018).
- [14] B. Singh, M. K. Gupta, S. K. Mishra, R. Mittal, P. U. Sastry, S. Rols, and S. L. Chaplot, Anomalous lattice behavior of vanadium pentoxide (V_2O_5): X-ray diffraction, inelastic neutron scattering and *ab initio* lattice dynamics, *Phys. Chem. Chem. Phys.* **19**, 17967 (2017).
- [15] E. Londero and E. Schröder, Vanadium pentoxide (V_2O_5): A van der waals density functional study, *Comput. Phys. Commun.* **182**, 1805 (2011).
- [16] E. Londero and E. Schröder, Role of van der waals bonding in the layered oxide V_2O_5 : First-principles density-functional calculations, *Phys. Rev. B* **82**, 054116 (2010).
- [17] S. Sucharitakul, G. Ye, W. R. L. Lambrecht, C. Bhandari, A. Gross, R. He, H. Poelman, and X. P. A. Gao, V_2O_5 : A 2D van der waals oxide with strong in-plane electrical and optical anisotropy, *ACS Appl. Mater. & Inter.* **9**, 23949 (2017).
- [18] N. Kenny, C. Kannewurf, and D. Whitmore, Optical absorption coefficients of vanadium pentoxide single crystals, *J. Phys. Chem. Solids* **27**, 1237 (1966).
- [19] C. Songhee, S. Jaeseok, O. Junhyeob, L. Ji-Hyun, J. J. Hyuck, and L. Shinbuhm, Sharp contrast in the electrical and optical properties of vanadium Wadsley (V_mO_{2m+1} , $m > 1$) epitaxial films selectively stabilized on (111)-oriented Y-stabilized ZrO_2 , *Phys. Rev. Mater.* **3**, 063401 (2019).
- [20] A. Othonos, C. Christofides, and M. Zervos, Ultrafast transient spectroscopy and photoluminescence properties of V_2O_5 nanowires, *Appl. Phys. Lett.* **103**, 133112 (2013).
- [21] Q.-H. Wu, A. Thissen, W. Jaegermann, M. Schütz, and P. Schmidt, Resonant photoemission spectroscopy study of electronic structure of V_2O_5 , *Chem. Phys. Lett.* **430**, 309 (2006).
- [22] R. J. O. Mossaneck, A. Mocellin, M. Abbate, B. G. Searle, P. T. Fonseca, and E. Morikawa, Cluster model and band structure calculations of V_2O_5 : Reduced V^{5+} symmetry and many-body effects, *Phys. Rev. B* **77**, 075118 (2008).
- [23] D. O. Scanlon, A. Walsh, B. J. Morgan, and G. W. Watson, An *ab initio* study of reduction of V_2O_5 through the formation of oxygen vacancies and Li intercalation, *J. Phys. Chem. C* **112**, 9903 (2008).
- [24] E. M. Roginskii, M. B. Smirnov, K. S. Smirnov, R. Baddour-Hadjean, J.-P. Pereira-Ramos, A. N. Smirnov, and V. Y. Davydov, A computational and spectroscopic study of the electronic structure of V_2O_5 -based cathode materials, *J. Phys. Chem. C* **125**, 5848 (2021).
- [25] A. Jarry, M. Walker, S. Theodoru, L. J. Brillson, and G. W. Rubloff, Elucidating structural transformations in $Li_xV_2O_5$ electrochromic thin films by multimodal spectroscopies, *Chem. Mater.* **32**, 7226 (2020).
- [26] X. Liu, J. Zeng, H. Yang, K. Zhou, and D. Pan, V_2O_5 -based nanomaterials: synthesis and their applications, *RSC Adv.* **8**, 4014 (2018).
- [27] J. M. Cocciantelli, J. P. Doumerc, M. Pouchard, M. Broussely, and J. Labat, Crystal chemistry of electrochemically inserted $Li_xV_2O_5$, *J. Power Sources* **34**, 103 (1991).
- [28] D. W. Murphy, P. A. Christian, F. J. DiSalvo, and J. V. Waszczak, Lithium incorporation by vanadium pentoxide, *Inorg. Chem.* **18**, 2800 (1979).
- [29] R. Baddour-Hadjean, E. Raekelboom, and J. P. Pereira-Ramos, New structural characterization of the $Li_xV_2O_5$ system provided by raman spectroscopy, *Chem. Mater.* **18**, 3548 (2006).
- [30] A. Talledo and C. G. Granqvist, Electrochromic vanadium-pentoxide-based films: Structural, electrochemical, and optical properties, *J. Appl. Phys.* **77**, 4655 (1995).
- [31] C. Sanchez, M. Henry, R. Morineau, and M. C. Leroy, Small polaron mobility in α - LiV_2O_5 , *Phys. Status Solidi B* **122**, 175 (1984).
- [32] B. Pecquenard, D. Gourier, and D. Caurant, Electron nuclear double resonance of polarons in α - $Li_xV_2O_5$, *J. Phys. Chem.* **100**, 9152 (1996).
- [33] P. Wathaisong, S. Jungthawan, P. Hirunsit, and S. Suthirakun, Transport properties of electron polarons in a V_2O_5 cathode of Li-ion batteries: A computational study, *RSC Adv.* **9**, 19483 (2019).

- [34] S. Suthirakun, A. Genest, and N. Rösch, Modeling polaron-coupled Li cation diffusion in V_2O_5 cathode material, *J. Phys. Chem. C* **122**, 150 (2018).
- [35] A. I. Liechtenstein, V. I. Anisimov, and J. Zaanen, Density-functional theory and strong interactions: Orbital ordering in Mott-Hubbard insulators, *Phys. Rev. B* **52**, R5467 (1995).
- [36] G. Kresse and J. Furthmüller, Efficient iterative schemes for *ab initio* total-energy calculations using a plane-wave basis set, *Phys. Rev. B* **54**, 11169 (1996).
- [37] G. Kresse and J. Hafner, *Ab initio* molecular-dynamics simulation of the liquid-metal–amorphous-semiconductor transition in germanium, *Phys. Rev. B* **49**, 14251 (1994).
- [38] J. P. Perdew, K. Burke, and M. Ernzerhof, Generalized gradient approximation made simple, *Phys. Rev. Lett.* **77**, 3865 (1996).
- [39] S. Grimme, Semiempirical GGA-type density functional constructed with a long-range dispersion correction, *J. Comput. Chem.* **27**, 1787 (2006).
- [40] S. Grimme, A. Hansen, J. G. Brandenburg, and C. Bannwarth, Dispersion-corrected mean-field electronic structure methods, *Chem. Rev.* **116**, 5105 (2016).
- [41] H. Park, R. Nanguneri, and A. T. Ngo, DFT + DMFT study of spin-charge-lattice coupling in covalent $LaCoO_3$, *Phys. Rev. B* **101**, 195125 (2020).
- [42] A. T. Lee, H. Park, and S. Ismail-Beigi, Origin of the orbital polarization of Co^{2+} in La_2CoTiO_6 and $(LaCoO_3)_1 + (LaTiO_3)_1$: A DFT + U and DMFT study, *Phys. Rev. B* **103**, 125105 (2021).
- [43] V. Singh, U. Herath, B. Wah, X. Liao, A. H. Romero, and H. Park, DMFTwDFT: An open-source code combining dynamical mean field theory with various density functional theory packages, *Comput. Phys. Commun.* **261**, 107778 (2021).
- [44] A. A. Mostofi, J. R. Yates, Y.-S. Lee, I. Souza, D. Vanderbilt, and N. Marzari, Wannier90: A tool for obtaining maximally-localised Wannier functions, *Comput. Phys. Commun.* **178**, 685 (2008).
- [45] A. Georges, G. Kotliar, W. Krauth, and M. J. Rozenberg, Dynamical mean-field theory of strongly correlated fermion systems and the limit of infinite dimensions, *Rev. Mod. Phys.* **68**, 13 (1996).
- [46] K. Haule, Exact double counting in combining the dynamical mean field theory and the density functional theory, *Phys. Rev. Lett.* **115**, 196403 (2015).
- [47] J. C. Slater, Magnetic effects and the Hartree-Fock equation, *Phys. Rev.* **82**, 538 (1951).
- [48] J. Kanamori, Electron correlation and ferromagnetism of transition metals, *Prog. Theor. Phys.* **30**, 275 (1963).
- [49] A. Georges, L. d. Medici, and J. Mravlje, Strong correlations from Hund's coupling, *Annu. Rev. Condens. Matter Phys.* **4**, 137 (2013).
- [50] H. Park, A. J. Millis, and C. A. Marianetti, Computing total energies in complex materials using charge self-consistent DFT + DMFT, *Phys. Rev. B* **90**, 235103 (2014).
- [51] V. M. Galitskii and A. B. Migdal, Application of quantum field theory methods to the many body problem, *J. Expt. Theor. Phys.* **34**, 139 (1958).
- [52] X. Wang, M. J. Han, L. de' Medici, H. Park, C. A. Marianetti, and A. J. Millis, Covalency, double-counting, and the metal-insulator phase diagram in transition metal oxides, *Phys. Rev. B* **86**, 195136 (2012).
- [53] M. Jarrell and O. Biham, Dynamical approach to analytic continuation of quantum Monte Carlo data, *Phys. Rev. Lett.* **63**, 2504 (1989).
- [54] V. Eyert and K.-H. Höck, Electronic structure of V_2O_5 : Role of octahedral deformations, *Phys. Rev. B* **57**, 12727 (1998).
- [55] T. K. Le, M. Kang, S. W. Han, and S. W. Kim, Highly intense room-temperature photoluminescence in V_2O_5 nanospheres, *RSC Adv.* **8**, 41317 (2018).
- [56] A. E. Bocquet, T. Mizokawa, K. Morikawa, A. Fujimori, S. R. Barman, K. Maiti, D. D. Sarma, Y. Tokura, and M. Onoda, Electronic structure of early $3d$ -transition-metal oxides by analysis of the $2p$ core-level photoemission spectra, *Phys. Rev. B* **53**, 1161 (1996).
- [57] K. W. Goodman and V. E. Henrich, Assignment of a photoemission feature in the O-2s–O-2p band gaps of TiO_2 and V_2O_5 , *Phys. Rev. B* **50**, 10450 (1994).
- [58] V. A. Ioffe and I. B. Patrino, Comparison of the small-polaron theory with the experimental data of current transport in V_2O_5 , *Phys. Status Solidi B* **40**, 389 (1970).
- [59] H. Giannetta, C. Calaza, D. Lamas, L. Fonseca, and L. Fraigi, Electrical transport properties of V_2O_5 thin films obtained by thermal annealing of layers grown by RF magnetron sputtering at room temperature, *Thin Solid Films* **589**, 730 (2015).
- [60] A. D. Becke and K. E. Edgecombe, A simple measure of electron localization in atomic and molecular systems, *J. Chem. Phys.* **92**, 5397 (1990).
- [61] B. Silvi and A. Savin, Classification of chemical bonds based on topological analysis of electron localization functions, *Nature (London)* **371**, 683 (1994).
- [62] A. Ormeci, H. Rosner, F. R. Wagner, M. Kohout, and Y. Grin, Electron localization function in full-potential representation for crystalline materials, *J. Phys. Chem. A* **110**, 1100 (2006).